ELSEVIER

Journal of Alloys and Compounds 293–295 (1999) 770–774

Journal of ALLOYS AND COMPOUNDS

Performance of an AB_2 alloy in sealed Ni–MH batteries for electric vehicles: quantification of corrosion rate and consequences on the battery performance

B. Knosp*, L. Vallet, Ph. Blanchard

SAFT Research Department, Route de Nozay, 91460 Marcoussis, France

Abstract

The purpose of this study is to evaluate the corrosion rate of a Laves phase alloy, with the C15 crystallographic structure, in 22 Ah sealed Ni–MH batteries for electric vehicle applications. At the end of life, measurements of the capacities of negative and positive electrodes show that the battery capacity is limited by the negative polarity. Negative electrodes exhibit a capacity loss of 60% which is attributed to kinetics problems due to the corrosion layers and to a loss of the active material. A model allowing the determination of the alloy corrosion has been developed by taking into account the solubilities and the oxidation state of the corrosion products and the amount of oxygen in corroded alloy. Although the corrosion rate of the AB_2 alloy is equivalent to what has been observed using AB_5 alloys, its consequences on battery performance are more severe due to the high oxidation state of V and Zr.

Keywords: AB_2 alloys; Laves phases; Ni–MH battery; Corrosion; Cycle life

1. Introduction

The range of electric vehicles (EV) is limited by the specific energy of batteries used as power sources. Due to their better performances than the currently used lead–acid or Ni–Cd systems, Ni–MH batteries constitute one of the most promising power sources for EVs in the near future and are the object of intensive developments.

At the present time the most widely studied alloys belong to the AB_5 group. Hydrogen storage capabilities of these alloys (300 mAh g^{-1}) make possible the manufacture of 70 Wh kg^{-1} batteries but can hardly go beyond. It has been also shown that the end of life of these batteries comes from the alloy corrosion which causes an increase of the inner pressure, an increase of the impedance and leads to H_2 venting [1,2].

In order to develop 80 Wh kg^{-1} batteries, intensive research work was focused on a new generation of alloys with specific capacities close to 400 mAh g^{-1}, such as $Zr(Ni, Mn)_2$ Laves phases [4–7]. Acceptable cycle life has been obtained using cubic C15 Laves phases with capacities over 370 mAh g^{-1}. Moreover, 22 Ah Ni–MH sealed batteries for EV application, using an AB_2 alloy as negative active material, exhibited a capacity loss lower than 30% after 575 cycles, but these performances still need to be improved [8].

So, in view of what has been already observed with AB_5 alloys, the first purpose of this work was to evaluate the alloy corrosion. The second purpose was to investigate the mechanisms of the end of life of the AB_2-based Ni–MH batteries. Particularly, the consequences of the alloy corrosion on the electrolyte consumption and change in the balance between positive and negative polarities have been evaluated.

2. Experimental details

2.1. Battery assembling and testing

Positive limited prismatic 22 Ah sealed cells were assembled using a cubic C15 Laves phase alloy $ZrNi_{1.2}Mn_{0.6}V_{0.2}Cr_{0.05}Co_{0.05}$ as active material in the negative electrodes as previously described [8]. A ternary mixture of KOH, NaOH and LiOH in 8.5 M aqueous solution was used as electrolyte. Pressure built up during cycling was monitored.

After 20 cycles of electrical activation, cycle life tests were performed at C/3 rate at 80% DOD. Capacities were

*Corresponding author.

0925-8388/99/$ – see front matter
PII: S0925-8388(99)00460-0

measured at C/3 discharge rate after a C/5 charge for 5 h followed by a 4 h overcharge at the C/20 rate.

2.2. Disassembling of the batteries

Before disassembling, gas evolved during the charge was analysed using gas chromatography. The batteries were disassembled in the discharged state. Negative and positive electrode samples from the stack were used for electrochemical tests.

Other positive electrodes and the separator, assigned to chemical analyses, were immersed separately in a mixture of nitric and hydrochloric acids.

To prevent the AB_2 alloy from burning, the negative electrodes were washed until pH 7, dried at 70°C under argon gas, then passivated under 20–50 vpm oxygen containing argon gas.

2.3. Electrochemical characterisation of the electrodes from disassembled cells

Negative and positive electrodes were tested in flooded cells for electrochemical characterisation. Charge and discharge rates used for this characterisation are based on the rated capacity of one positive electrode (1.8 Ah).

Each sample electrode was assembled in an open cell with previously charged counter electrodes in excess. The cells were discharged at C/3 rate in order to measure the non-discharged capacity in sealed conditions. The total capacity of these electrodes was measured using a charge at C/10 rate with 25% overcharge (based on their rated capacity) followed by a discharge performed at C/3 and then at C/10 rate, to cut-off voltage 0.9 V.

2.4. Chemical characterisations of the electrodes

Corrosion products in passivated negative electrodes were characterised using X-ray diffraction (XRD), scanning electron microscopy (SEM) and semiquantitative energy dispersive X-ray spectroscopy (EDX). Alloy powder was extracted out of negative electrodes using an ultrasonic apparatus and its oxygen content was measured with a LECO apparatus. The samples react with a carbon crucible at 2000°C and yield CO_2, which is analysed by selective infrared absorption.

Positive electrodes or separator were dissolved in a boiling mixture of nitric and hydrochloric acids. Then, the obtained solution was filtered and analysed using inductively coupled plasma (ICP) spectroscopy.

3. Results

3.1. Cycle life test

The capacity and the inner pressure at the end of charge of the 22 Ah sealed batteries as a function of cycle number are shown in Fig. 1. The capacity, which reaches 23 Ah after activation, remains over 19 Ah during 575 cycles, which represents a capacity loss lower than 20%. A progressive increase of the pressure at the end of charge is observed during ~250 cycles. This pressure increase is due to H_2 gas evolution, as determined by gas chromatography analysis. At the end of life, hydrogen venting occurs through opening of the pressure valve.

Hydrogen venting has already been observed at the end of life of sealed MH batteries with AB_5 alloys and was explained by corrosion of alloy in electrolyte [1].

3.2. Electrochemical characterisations

The non-discharged capacities in sealed conditions were found to be 0.38 Ah for positive electrodes (whatever their location in the stack) while they range between 0 Ah (in the centre of the stack) and 0.25 Ah (for external plates) for the negative electrodes. This variation throughout the stack is assumed to come from the temperature distribution in the battery. Nevertheless, it appears that the discharge of

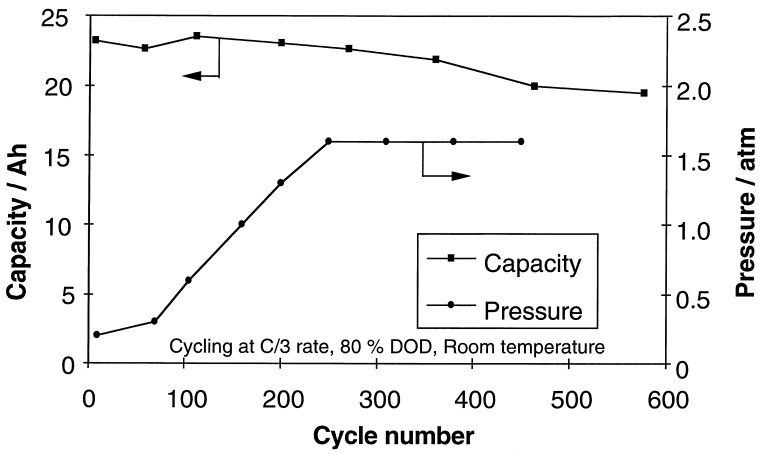

Fig. 1. Evolution of the capacity and the inner pressure at the end of charge during cycling of 22 Ah sealed cells.

Table 1
Fraction (%) of the alloy components outside the negative stack determined using ICP analysis

Component	V	Mn	Co	Cr	Zr	Ni
Separator	2.51	0.83	2.59	3.82	0.06	1.5
Positive electrode	5.5	3.23		1.17	0.13	
Total	8.1	4.1	2.6	5.0	0.2	1.5

the batteries at the end of life is limited by the negative polarity.

Besides, positive electrodes exhibit total capacities slightly higher than their rated capacity, using a C/3 discharge rate. On the other hand, it has been found that the negative electrodes lose ~60% of their rated capacity after cycling. Moreover, less than 80% of the remaining capacity was discharged at C/3 rate, the remaining capacity is measured at C/10 rate, which indicates kinetic limitations.

So, it can be concluded that the cycle life of the battery is limited by the capacity loss of the negative electrode, which results probably not only from a decrease of active material due to the alloy corrosion but also partly from kinetic limitations.

3.3. Chemical characterisations

The amount of the alloy components in the separator and in positive electrodes were determined by ICP chemical analysis. The results described in Table 1 (as Ni and Co are the constituents of the positive active material, their contents in positive electrodes do not represent alloy corrosion and were not measured) show that the alloy components dissolve in the electrolyte, but measured amounts ($\leq$8% of the bulk composition) cannot explain the capacity loss of the negative electrodes.

SEM observations of negative electrodes cross-sections showed a layer of corrosion products around the alloy particles, which could explain the kinetic limitation observed.

Despite the small size of alloy particles and corroded surface, the ratios Zr/Ni, Mn/Ni and V/Ni were determined using semi-quantitative EDX analysis. The ratios in corrosion products are ~40% lower than in the alloy. This result confirms that a part of the alloy is dissolved during the corrosion process.

XRD diagrams obtained on cycled negative electrodes show weak peaks in addition to the peaks of the alloy. These peaks could be attributed to oxides (probably partly due to dehydrated hydroxides or oxidised nanometric metal particles during the passivation treatment). The oxides identified are: $Co_2V_2O_7$, ZrO_2, Mn_2O_3, Mn_3O_4, $Co_2Mn_3O_8$ and $(Co,Mn)(Mn,Co)_2O_4$. From these results, the oxidation states of the alloy components in the corrosion products are +5 for V, +4 for Zr, +3 (mean value) for Mn and +2 for Co. On the other hand, no peak corresponding to chromium oxide was observed (probably Cr_2O_3 was not detected due to the low Cr content in the alloy) nor for nickel oxide (probably because the more intense peaks of NiO interfere with peaks of the alloy).

Finally, a content of 9 wt.% of oxygen has been found in the corroded alloy powder extracted from the passivated negative electrodes.

4. Discussion

4.1. Evaluation of corrosion rate

The major components of the AB_2 alloy (excluding Ni which is also a major component of the positive active material) were found not only in the positive electrodes but also in the corroded layer of the alloy and cannot be used as a corrosion tracer like aluminium contained in AB_5 alloys, which is entirely trapped in the positive electrode [3].

In order to evaluate the corrosion rate of the AB_2 alloy, a model, schematically presented in Fig. 2, is proposed using the following assumptions: (i) the corrosion rate *x* is the same for all the alloy components; (ii) all the corrosion

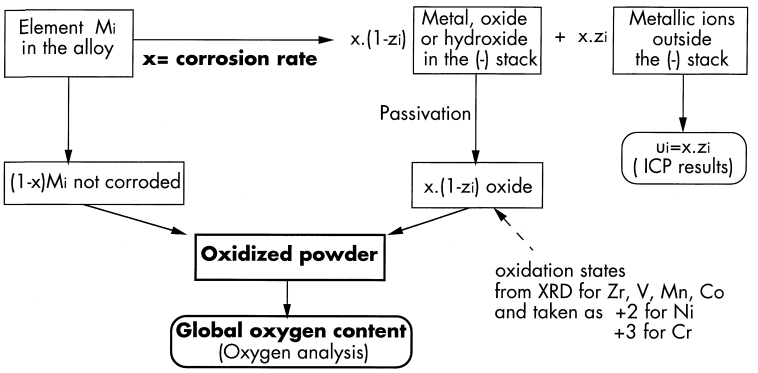

Fig. 2. Model used to determine the alloy corrosion rate *x* from oxygen content of corroded powder and fractions u_i of the alloy components found outside the negative stack (z_i = eluted fraction of the corroded product of element i).

products remaining in the passivated negative electrodes are oxides; (iii) the oxygen content of the corroded alloy originates from corrosion products in the negative electrode; (iv) the oxidation states of the components are those previously mentioned, and taken as +3 for Cr and +2 for Ni; (v) the ratio between the eluted fractions z_i of the corrosion products are proportional to their total amount u_i found outside the negative electrodes using ICP analysis (see Table 1).

Assuming that u_i can accurately be measured using ICP spectroscopy, this model allows to calculate the oxygen content of the corroded powder as a function of the corrosion rate (Fig. 3). From this figure it is found that the oxygen content (9%) corresponds to a corrosion rate of 28%, equivalent to what is observed using AB_5 alloys [2].

However, this result cannot fully explain the capacity loss of the negative electrodes and confirms the existence of a kinetic limitation due to the layer of corrosion products observed using SEM.

4.2. Consequences of corrosion on the battery performance

Because of the passivation treatment applied on cycled negative electrodes prior to analysis, corrosion products formed in the battery cannot be precisely determined. Therefore, corrosion of AB_2 alloy could proceed as:

$$M + nH_2O \rightarrow M(OH)_n + nH_{ads}$$

or

$$M + n/2H_2O \rightarrow MO_{n/2} + nH_{ads}.$$

In both cases, the alloy corrosion leads to (i) water consumption, which contributes to a drying out of the separator; (ii) a decrease of the quantity of negative active material; (iii) a production of hydrogen, which is absorbed by the hydrogen storage alloy. This leads to a spontaneous creation of negative discharge reserve and decreases the negative charge reserve. When the charge reserve becomes insufficient, hydrogen gas evolution occurs at the end of charge [1,2], and the inner pressure increases during cycling as seen in Fig. 1.

Assuming that Co and ~80% of Ni of the alloy are not oxidised in the battery (as done in Ref. [2] for AB_5 alloys), water consumption ranges from 0.32 cm^3 (formation of oxides) to 0.64 cm^3 (hydroxides) per gram of corroded AB_2 alloy, which compares to a typical value of 0.3 cm^3 for AB_5 alloys.

Taking into account the alloy composition and oxidation states mentioned above, the negative discharge reserve is increased by 950 mAh/g of corroded AB_2 alloy. This is approximately twice the increase of discharge reserve observed when 1 g of AB_5 alloy is corroded [2].

5. Conclusions

The capacity loss of 22 Ah Ni–MH sealed cells for EV applications using an AB_2 alloy as a negative active material is lower than 20% after 575 cycles.

The cycle life of the batteries is related to the capacity loss of the negative electrode, because of active material loss and kinetic problems.

The corrosion rate of AB_2 alloys (≈28%) is nearly equivalent to that previously measured on AB_5 alloys, but its consequences on the water consumption and negative discharge reserve are more severe for AB_2 alloys, due to the high oxidation states of Zr (+4) and V (+5) in the corrosion products.

As a consequence, in order to achieve the same level of performances as AB_5-based NiMH batteries, AB_2 alloys must exhibit half the corrosion rates of AB_5 alloys.

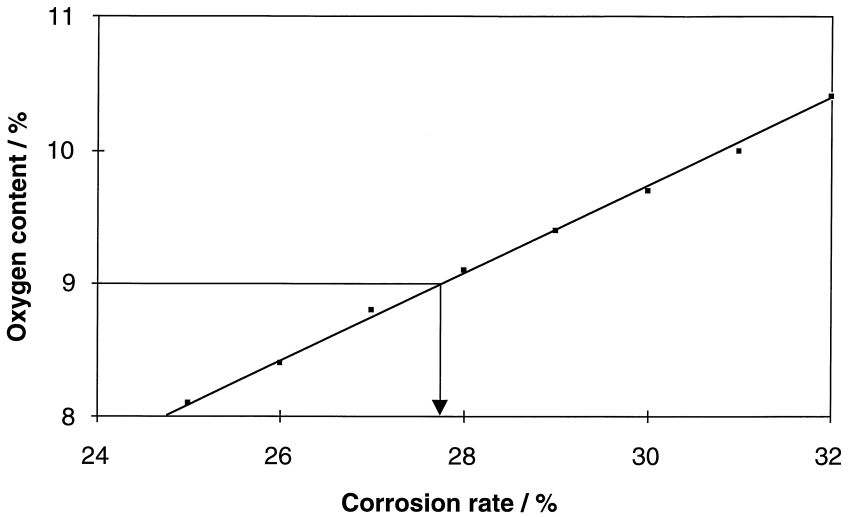

Fig. 3. Oxygen content calculated as a function of the corrosion rate using the model.

References

[1] H. Kaiya, T. Ookawa, J. Alloys Comp. 232 (1995) 598.
[2] P. Leblanc, C. Jordy, B. Knosp, Ph. Blanchard, J. Electrochem. Soc. 145 (1998) 860.
[3] P. Bernard, J. Electrochem. Soc. 145 (1998) 456.
[4] Y. Moriwaki, T. Gamo, H. Seri, T. Iwaki, J. Less Common Metals 172–174 (1991) 1211.
[5] T. Gamo, Y. Tsuji, Y. Moriwaki, in: P. Bennet, T. Sakai (Eds.), Hydrogen and Metal Hydride Batteries, The Electrochemical Society Proceedings Series, The Electrochemical Society, New Jersey, 1994, p. 155, PV 94-27.
[6] J. Bouet, B. Knosp, A. Percheron-Guégan, O. Canet, European Patent EP-B-0 587 503 (1997).
[7] B. Knosp, M. Mimoun, J. Bouet, D. Gicquel, C. Jordy, European Patent Application EP A-0 677 881 (1995).
[8] B. Knosp, C. Jordy, Ph. Blanchard, T. Berlureau, J. Electrochem. Soc. 145 (1998) 1478.